On Slope Winds

by
Li Peng

ABSTRACT

The equations of shallow convection are applied to the investigation of the circulations in a stable atmosphere above a V-shaped valley. For simplicity, the motion is assumed to be uniform along the valley and symmetric about the vertical planes passing through valley-and ridge-axis. The heating or cooling of the sloping ground is simulated by prescribing the variations of ground temerature. Two numerical integrations of the equations have been carried out for upslope-and downslope-winds separately. The results show that:

a) the peak intensity of the circulation in daytime leads the maximum ground temperature nearly two hours;

b) the highest upslope velocity occurs above the upper half of the slope at a definite distance less than fifty meters from the slope and maximum vertical velocity is directly above the ridge;

c) the thickness of the upslope winds is within the range of 100 to 200 meters, changing accordingly with the intensity of the circulation;

d) in the early stage of the development of the upslope winds, the potential energy of the system increases with time because of subscale diffusion process, but after the slope wind is fully developped, it decreases with time mainly due to subscale diffusion, only a small portion of the reduction is transformed into kinetic energy;

e) the nighttime downslope wind is much weaker and shallower and reaches its maximum intensity much faster than the daytime upslope wind;

f) the returning flow is much weaker but of greater thickness than the slope wind. These results are in good agreement with observations summarized in Defant's review article (Defant, 1951) and Geiger's book (Geiger, 1957).

1. Introduction

The topographical variations of a mountainous terrain exert inportant influences on the local climate. Particularly, the inclined mountain slopes act as heat sources in daytime and heat sinks in nighttime and, consequently, generate diurnal variations in solenoidal field and local circulation. According to the observations summarized in Defant's review article (Defant, 1951) and Geiger's book (Geiger, 1957), the winds blow uphill in daytime, start about a half hour after sunrise, reach their greatest intensity at the time of maximum insolation, and reverse their direction in the evening. The thickness of the slope wind layer generally lies between 100 and 200 meters, and, on the average, the slope wind speeds amount to about 2 to 4m/sec according to measurements. The highest velocity does not occur close to the slope surface but at a definite distance from it. Higher up, it rapidly decreases again.

A theoretical account for thermal slope winds was first given by Prandtl in 1942 (see Defant, 1951). He considered an inclined slope of infinite extent on which the deviation of potential temperature from a level stratification is only a function of the distance normal to the slope, so that the problem was made one-dimensional and linear. The steady solution of this simplified problem found by Prandtl, in terms of the angle of inclination, the stability,

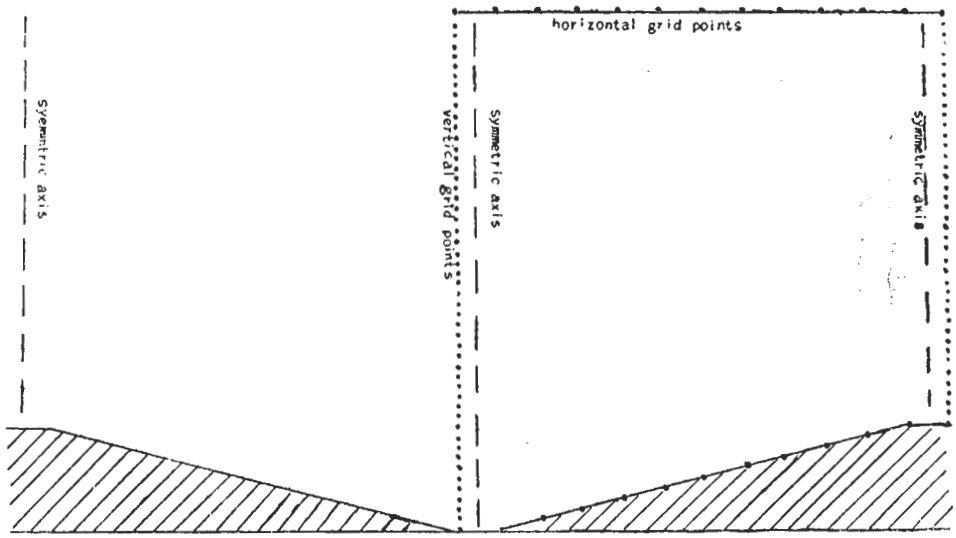

Fig. 1. Mountain-valley profile.
山一谷剖影圖

and the coefficients of heat conduction and turbulent friction, well explained the variation of slope winds in the direction normal to the slope. Later Defant extended Prandtl's steady solution to include the time-oscillatory nature by simply multiplying, as a first approximation, the steady solution by the factor $\cos\Omega t$. Because of their lineir and one-dimensional nature, Prandtl's and Defant's solutions can not account for the detailed structure of the thermal circulations on natual slopes of finite length, especially the variations of wind and temperature along the slopes which evidently are very important to microclimatology.

A numerical study of thermal upslope winds were made by Thyer and Buettuer (1962) as part of their study of mountain-valley winds in the V-shaped valley. However, they encountered the dificulties of computational instability and were unable to integrate the equations beyond two minutes. Orville (1964) used the mountain-plain profile consisting of a mountain of 1 km high with a 45° slope and a level plain 2 km long extending from the base of the mountain. Two cases of upslope winds were studied, one in a neutral environment, the other in a slightly stable environment. Respectively a bubble and a columnar shaped convection were formed over the mountain slope. Both integrations were terminated before the caps of the respective rising bubble and column over the mountain nearly reached the solid upper boundary.

The main purpose of the present paper is to present some results of numerical simulation of the evolution of thermal slope winds. The investigation represents partial results in a continual study of orographical infiuences on local circulations and airflows. In order to achieve long time-integration enough to show the evolution of thermal slope winds, we consider an atmosphere of normal stratification above a mountain slope of gentle inclination. The results are to be compared with observations and previous numerical experiments.

2. The model

2.1. The equations

The equations used in the model are the following:

$$\frac{\partial \eta}{\partial t} = -J(\psi,\eta) + \frac{g}{\theta}\frac{\partial \theta'}{\partial y} + K_H\frac{\partial^2 \eta}{\partial y^2} + K_z\frac{\partial^2 \eta}{\partial z^2} \quad (1)$$

$$\frac{\partial\theta'}{\partial t} = -J(\psi,\theta') + K_H\frac{\partial^2\theta'}{\partial y^2} + k_z\frac{\partial^2\theta'}{\partial z^2} \quad (2)$$

$$\eta = \frac{\partial^2\psi}{\partial z^2} + \frac{\partial^2\psi}{\partial y^2} \quad (3)$$

where η is vorticity, ψ is stream function, θ is potential temperature deviation from a reference state, Θ, g is the acceleration of gravity, K_H and K_z are respectively the horizontal and vertical eddy coefficients for both momentum and heat diffusion, J is the Jacobin with respect to y and z. In these equatione, the Coriolis effect is neglected because of small horizontal scale. All x-derivatives are also neglected by assuming that the mountain ranges are very long in the x-direction. These equations are the same as those in Orville's model. They are solved numerically under the boundary and initial conditions to be given below. The velocity components in the y-and z-direction may be obtained by

$$v = -\frac{\partial\psi}{\partial z} \quad \text{and} \quad w = \frac{\partial\psi}{\partial y} \quad (4)$$

respectively.

2.2. Mountain-valley profile and boundary conditions

We consider an east-west oriented valley with the cross-valley profile shown in Fig. 1. Reflective symmetry about the vertical plane through the valley axis is assumed so that the solution in the right half plane is just the mirror image of the left. To cover one half domain in the Y-Z plane, we use M+2 equally spaced (δy) grids in the cross-valley direction and N+1 equally spaced (δz) grids in the vertical. The grid distances are so chosen that the ratio $\delta z/\delta y$ is equal to the slope of the mountain and that the mountain top is (M-1)δz above the valley floor.

For the upper boundary conditions, we assume that at a sufficient height above the ground all perturbations are negligible.

$$\eta = \psi = 0, \text{ and } \theta' = \text{cconstant at } z = Z. \quad (5)$$

Along the lateral boundaries, reflective symmetry is assumed. In other words,

$$\theta'_{1K} = \theta'_{2K},\ \psi_{1K} = -\psi_{2K},\ \eta_{1K} = -\eta_{2K} \quad (6)$$

$$\theta'_{NK} = \theta'_{NHK},\ \psi_{NK} = -\psi_{N+1K},\ \eta_{NK} = -\eta_{N+1K} \quad (7)$$

for all k. Along the ground surface,

$$\psi = 0 \quad (8)$$

The potential temperature change at the ground surface is the driving agent of the motion and is specified as follows.

$$\theta' = \bar{\theta}(z) + (\theta^* - \alpha z)\sin\frac{\pi(t-\lambda)}{43200} \text{ at } z = z_g \quad (9)$$

where the first part is the initial temperature stratification and the second part represents the diurnal change (t is time in seconds). Vorticities at the gound are predicted by Eq. (1) using the diference schemes in 2.4.

2.3 Energy equations

Multiplying Eq. (1) by $-\psi$, Eq. (2) by $-gz/\Theta$, and integrating the resultant equations over the domain shown in Fig. (1), we have, after making use of the boundary conditions Eqs. (5)-(8),

$$-\frac{d}{dt}\int\int\rho_0\frac{v^2+w^2}{2}dydz = C - D \quad (10)$$

and

$$-\frac{d}{dt}\int\int\rho_0\frac{-gz\theta'}{\Theta}dydz = -C + F \quad (11)$$

where

$$C = \frac{\rho_0 g}{\Theta}\int\int\theta' w dydz \quad (12)$$

$$D = \int\int\rho_0\{K_H[(\frac{\partial v}{\partial y})^2 + (\frac{\partial v}{\partial z})^2] + K_z[(\frac{\partial w}{\partial y})^2 + (\frac{\partial w}{\partial z})^2]\}dydz \quad (13)$$

$$F = B_H - B_G + B_{top} + G \quad (14)$$

$$B_H = -\frac{g}{\Theta}\int_0^{Z_G}K_H(z\frac{\partial\theta'}{\partial z})\text{slope}\rho_0 dz \quad (15)$$

$$B_G = -\frac{g}{\Theta}\int(K_z\frac{\partial z\theta'}{\partial z})_{z_g}\rho_0 dy \quad (16)$$

$$B_{top} = -\frac{g}{\Theta}\int(K_z\frac{\partial z\theta'}{\partial z})_z\rho_0 dy \quad (17)$$

$$G = \frac{2g}{\Theta}\int\rho_0 K_z(\theta_z - \theta_{zg})dy \quad (18)$$

Z_G is the height of mountain peak, and ρ_0 is the mean density in the domain. Combining Eqs. (10) and (11), we have

$$\frac{d}{dt}\int\int\rho_0\left(\frac{v^2+w^2}{2}+\frac{-gz\theta'}{\Theta}\right)dydz=F-D \quad (19)$$

Clearly, the left hand side of Eq. (10) is the total ketinic energy, D, kinetic energy dissipation, C, conversion from potential to kinetic energy, $-gz\theta'/\Theta$, the potential energy in the system, and B_H, B_σ, B_{top} and G, all due to subscale diffusion process, are respectively horizontal fluxes from the lower boundary, upward flux at the top and the generation of potential energy within the domain. If K_H and K_Z are set equal to zero, the total of kinetic and potential energy will be conserved.

2.4. Finite difference schemes

a. Space difference scheme. At interior grid points, the buoyancy and diffusion terms in Eqs. (1)—(2) are computed by centered difference scheme. At the lower boundary points, the buoyancy term is approximated by one-side differencing and the diffusion terms are approximated by 2Grad/δ where Grad stands for one-side gradient of η θ' and δ for δy or δz. For the Jacobian in Eq. (2), we use

$$J_{j,k}(\psi,\theta)=\{(\psi_{j+1,k}-\psi_{j,k+1})\theta'_{j+1,k+1}+(\psi_{j-1,k}-\psi_{j,k-1})\theta'_{j-1,k-1}-(\psi_{j-1,k}-\psi_{j,k+1})\theta'_{j-1,k+1}-(\psi_{j+1,k}-\psi'_{j,k-1})\theta'_{j+1,k-1}\}/4\delta y\delta z \quad (10)$$

and for the Jacobian in Eq. (1),

$$\begin{aligned}J_{j,k}(\psi,\eta)=\lambda\{&(\psi_{j+1,k}-\psi_{j,k+1})\eta_{j+1,k+1}+(\psi_{j-1,k}-\psi_{j,k-1})\eta_{j-1,k-1}-(\psi_{j-1,k}-\psi_{j,k+1})\eta_{j-1,k+1}-(\psi_{j+1,k}-\psi_{j,k-1})\eta_{j+1,k-1}-(\psi_{j,k+1}+\psi_{j+1,k+1}-\psi_{j,k-1}-\psi_{j+1,k-1})\eta_{j+1,k}\\&+(\psi_{j-1,k+1}+\psi_{j,k+1}-\psi_{j-1,k-1}-\psi_{j,k-1})\eta_{j-1,k}+(\psi_{j+1,k}+\psi_{j+1,k+1}-\psi_{j-1,k}-\psi_{j-1,k+1})\eta_{j,k+1}-(\psi_{j+1,k-1}+\psi_{j+1,k}-\psi_{j-1,k-1}-\psi_{j-1,k})\eta_{j,k-1}\}\\&/12\delta y\delta z \quad (11)\end{aligned}$$

where $\lambda=\begin{cases}1 & \text{at interion points}\\ 8/5 & \text{at the mountain top}\\ 2 & \text{along the mountain slope}\\ 8/3 & \text{at the bottom of the valley}\end{cases}$

and presumably η and ψ assume zero values at grids below the ground surface. The finite difference forms adopted for the Jacobians conserve the area integrals of θ', θ'^2, η, η^2 and kinetic energy in a closed domain if they are combined with forward time differencing (Arakawa, 1965).

b. Time difference scheme. Two finite difference schemes have been tried for upslope wind case, one, simple forward time difference, the other, Euler-backward. No significant differences were found before the calculations were terminated at t = 7 hr. For the downslope wind case, simple forward time difference was used.

2.5. Methed for solving Eq. (3)

Eq. (3) is directlysolved for ψ through the adjustment matrix which is defined as follows: For each n (n = 1,2,……, M), setting

$$\psi_{m,N+1}=0,\ m=1,2,\cdots\cdots,M,$$

and

$$\psi_{m,N}=\begin{cases}1 & \text{for } m=n,\\ 0 & \text{otherwise,}\end{cases}$$

we calculate the values of $\psi_{m,N-1}$, $\psi_{m,N-2}$, etc from $\frac{\partial^2\psi}{\partial y^2}+\frac{\partial^2\psi}{\partial z^2}=0$ and the laternal boundary conditions for ψ, and denote the obtained values of ψ at the ground grid points by $b_{m,n}$. Clearly, the set of $b_{m,n}$ for all n form a square matrix. It can be shown that this matrix has an inverse. We call the inverse the adjustment matrix and denote its element by $a_{m,n}$. To solve Eq. (3), we start with $\psi_{j,N+1}=\psi_{j,N}=0$, for j = 1 to M, and calculate from Eq. (3) and the boundary conditions Eqs. (6)-(7) the values of $\psi_{j,N-1}$, $\psi_{j,N-2}$, etc. Denote the values of ψ at the ground grids by R_j. If every R_j is zero or within a tolerable error limit, the calculated ψ is the solution. In general, this is not true and we must go back to adjust each $\psi_{j,N}$, to substract from it an amount of δ_j, say, in order that the new $\psi_{j,k}$ to be calculated in the same way will be the solution. It is readily seen that the required adjustments δ_j, j=1 to

M, must be the solution of

$b_{m,j}\delta_j = R_m$, to M.

Hence,

$\delta_j = a_{j,m}R_m$, j=1 to M.

Since the adjustment matrix is independent of η, we need to calculate it only once. This method, therefore, is far more economical than other iterative or relaxation methods. It came to our attention in the later stage of our study that this method was called "generalized sweep-out method" by Hirota et al (1970).

2.6. Initial conditions and parameters

The initial condition for potential temperature deviation is the following:

$\theta' = \theta'_0 + \gamma z = \bar{\theta}_{(s)}$, at t=0

where θ_0' and γ are contants. The initial vorticity field is zero everywhere, in other words, the atmosphere is at rest initially.

The parameters adopted are the following:

$\delta y = 250$m

$\delta z = 50$m

$\theta = 297°$K

$Z = 2500$m

M=11

N=50

$g = 9.8$m/sec

$K_z = 10$m^2/sec

$K_H = K_z(\delta y)^2/(\delta z)^2$

$\theta_0 = -4°$C

$\gamma = 0.004°$C/m

$\theta^* = 5°$C

$\alpha = 0.004°$C/m

$\lambda = 0$ for the case of upslope winds, 43200 for downslope winds

3. Results

3.1 Upslope winds

The initial conditions given in 2.6 approximate the state of atmosphere at 8:30 in the morning when the nighttime downslope winds have completely died out, the surface temperature inversion has disappeared and the stratification of the atmosphere has come close to the mean. Starting from the initial conditions, the set of equations given in section 2 has been integrated with $\lambda = 0$ for nearly seven hours of physical time. Fig. 2 shows the time variation of maximum horizontal velocity, which also represents the intensity change of the thermally induced circulation, for the vertical velocity is much smaller than the horizontal component. Clearly, upslope winds are built up as the temperature on the slope surface is increased by insolation. The wind reaches its peak value in about four hours, leading the maximum surface temperature almost 2 hours. The decaying stage takes less time than the developing. The evolution is in good agreement with the summary of observations mentioned in the introduction.

The thermal circulation starts with the center of streamlines located at the lower half of the slope. As intensifies continually, the center of streamlines moves up and away from the slope. It reaches the highesst position, 300 m above the slope, when the upslope wind down below attains the maximum intensity of 2.9 mps. Then it moves down and toward the slope, tending to complete a loop, (see Fig. 3). The upward part of the trajectory is similar to Orville's result in a slight stable atmosphere, where the streamline center ascended much faster and showed no tendency to move away from the ridge axis before the computation was terminated as the center came close to the upper boundary. These differences between Orville's and our results may be due to the fact the initial stratification is more stable and the mountain slope gentler in our model than in Orville's.

As the upslope wind intens-ifies, its thickness increases accordingly. As the wind weakens however, the thickness shrinks only slightly. This can be seen from Fig. 4 in which the vertical wind profile at the location of maximum upslope wind at 2hr, 4hr and 7hr are shown. It is also clear that above the layer of upslope winds there is a

layer of returning flow which is deeper in thickness but weak in intensity. Fig. 5 shows the time-height cross section of the shifts of horizontal wind direction above the fixed location two grids from the mountain peak. The lines indicate where the wind changes direction and the numbers, the maximum and minimum horizontal velocities in the vertical. The time variation of the thickness or upslope wind and returning flow are evident in the figure. Above the returning flow there exist still more oscillatory layers whose intensities are vanishingly weak though. The thickness of the upslope wind and the highest velocity agree very well with the observations cited in the introduction.

When the air near the sloping ground is heated and the thermal cirulation develops, heat energy is conducted upward by the circulation as well as subgrid diffusion. Consequently, potential temperature increases monotonically with time in the layer below 1500 m and gradually approaches a slight superadiabatic profile. This is clearly depicted in Fig. 6 where the potential temperature deviations above the valley and the mountain peak are plotted against the height. According to the energy equations, Eqs. (10)—(11), the upward transport of heat results in potential energy reduction, part of which is transfrmed into kinetic energy. Fig. 7 shows the time variation of calculated values of the terms in Eq. (11). Because of the over-all large static stability chosen in the model, the two biggest terms in the eqation are G and B_T. The resultant $G_I - B_T$ shown in the figure is positive only in the first hour, quickly becoming negetive and dominant. The horizontal component, B_H, of potential energy flux from the slope is the primary source of potential energy of the system. It supplies the energy being transformed into kinetic energy through the sinking of cooler air and rising of warming air. The vertical component of lower boundary flux is negative as long as the surface stratification remains stable. The total flux of potential energy from the ground, however, is positive till the end of computation. The curves of B and resultant $B_H + B_\sigma - B_T - G$ evidently indicate that the decrease of potential energy is due to the energy transformation C in the early half of computation but is dominated by the subgrid diffusion in the later half.

In order to give a better view of the structure of the upslope wind system, the streamline pattern, the horizontal and vertical velocities and the thermal structure at the time of maximum upslope wind are shown in Figs. 8—11 respectively. The thermal slope-circulation in a stable atmosphere is indeed a shallow phenomenon. The upslope windis even much more concentrated than the returning low. Its thichness varies only slightly but the velocity changes considerably along the slope. The highest speed is not located nearly half way on the slope but close to the mountain peak. The major portion of the upslope wind and the returning flow are parallel to the sloping ground. The upward motion is concentrated close to the ground and near the mountain peak, while the downward flow spreads atop over a much larger domain. Accordingly, the layer of unstable of unstable stratification is expanded considerably near the mountain peak but limited to a very shallow layer elswhere on the slope. The packing of isentropes due to the to the downward motion of the returning flow (see Fig. 11) is only very slight, unlike the unrealistic packing in Orville's result which was attributed by him to the assumption of a constant eddy coefficient.

3.2. Downslope winds.

The initial condions given in 2.6 also approximates the state of atmosphere at about two hours after sunset. Numerical integration

of the model equations has been carried out for slightly over five hours of physical time, starting from the initial conditions. For λ equal to a half day the second term on the right hand side of Eq. (9) simulates radiational cooling along the sloping ground. Because of the cooling, downslope motions are set up near the ground and a layer of returning flow appears atop as required by mass continuity. Some of the results are shown in Figs. 12—15. Evidently, the intensity of the downslope wind is much weaker than the upslope wind in the above mentioned case, and the thickness of the downslope wind and the returning flow are much shallower. Unlike the upslope-wind case, the downslope wind, as well as the returning flow, reaches its maximum intensity in less than two hours, than decreases steadily till the end of integration. These characteristics can be accounted for by the fact that the ground cooling greatly enhances the stable stratification of the stmosphere below 1.5 km, particularly, the surface layer (see Fig. 15).

4. Summary and concluding remarks.

The set of the equations of shallow water convection has been applied to the investigation of the evolution of thermally induced circulation above a V-shaped mountain-valley profile in a stable atmosphere. For simplicity, the motion is assumed to be uniform in the direction of valley axis and symmeric about the vertical plane passing through the axis of the valley as well as the mountain. The heating of cooling of the sloping ground is simulated by prescribing the diurnal variation of ground temperature. The major results of numerical integration of the equations may be summerized as follows:

a) The peak intensity of the thermally induced circulation in daytime leads the maximum surface temperature nearly two hours.

b) The highest upslope velocity occurs over the upper half of the slope at a distance of about fifty meters from the ground.

c) The thickness of the upslope wind is about 100 to 200 meters, changing accordingly with the intensity of the slope wind.

d) The returning flow is much weaker but of greater thickness than the slope wind.

e) The maximum vertical velocity is located above the mountain top.

f) In the first stage of the development of the upslope wind the potential enegy of the system increases because of subscale diffusion. After the upslope wind is fully developped, the potential energy decreases mainly due to subscale diffusion, only a small portion of it is transformed into kinstic energy.

g) The nighttime downslope wind is much weaker and shallower than the daytime upslope wind but attains its maximum intensity much faster. For the slope inclination of 1 to 5, the highest velocity is about 3 m/s for daytime upslope wind but less than 1 m/s for nighttime downslope winds.

Although the calculated results are in good agreement with observations, the model suffers from one major inadequacy, viz., atmospheric radiation effects, particularly during the night, is not taken into consideration in the model. Unless this shortcoming is corrected, it is not proper to carry out longer numerical integrations such as to investigate the diurnal cycle of thermally induced slope circulations. Other simplifications such as the motion being uniform in the direction of the valley axis and symmetric about the vertical plane passing through the axis of the valley as well as the mountain, should also be removed in order the results to be more realiestic.

Acknowledgments. The author is indebted to the National Science Counsel for support of the research. Thanks are due to Dr. W. Tang of Lowell Institute of Technology for helping

discussins, and Prof. Y. C. Kang of National Taiwan University and Dr. C. T. Wang of Academia Sinica for their encouragements.

REFERENCES

Arakawa, A., 1965: Computational design for long-term numerical integration of the equations of fluid motion: two dimensional incompressible flow. Part I. J. Compu. Phys. 1, 119-143.

Defant, F., 1951: Local winds. Compendium of meteorolgy. Amer. Meteor. Soc., 655-672.

Geiger, R., 1957: The climate near the ground. Harvard Univ. Press, 49pp.

Hirota,

Orville, H. D., 1964: On mountain upslope winds. J. Atmos. Sci., 21, 622-633.

Thyer, N. and K. J. K. Buettner, 1962: Part A: On valley and mountain winds III; Part B: Valley wind theory, Final Report, Univ. of Washington, AF Contract 19(604)-7201.

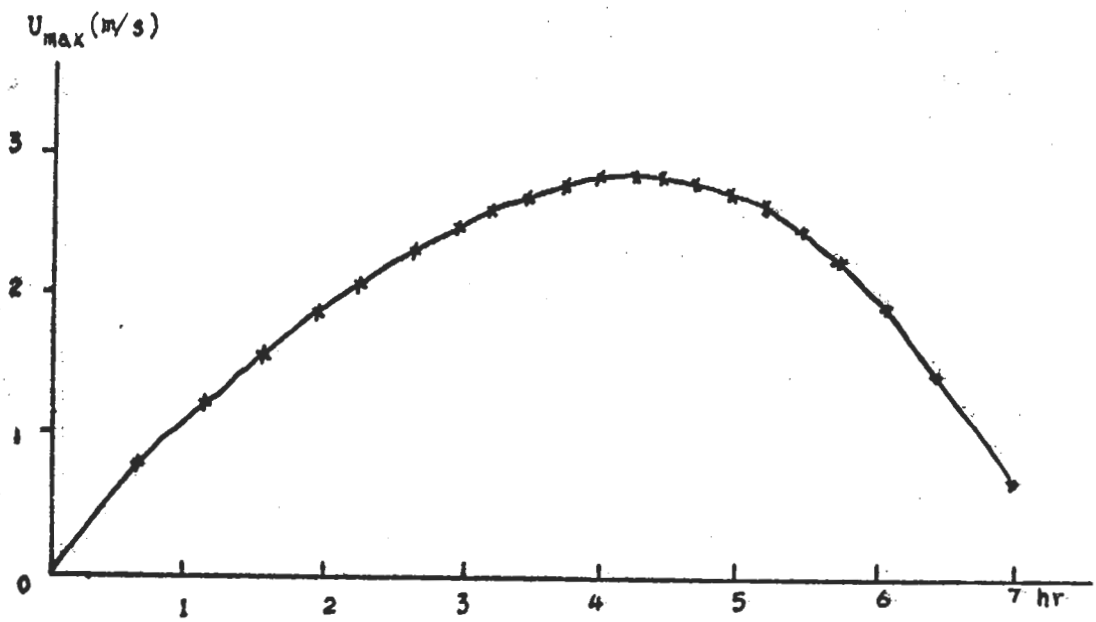

Fig. 2. Time variation of U_{max}.
U最大值之時間變化圖

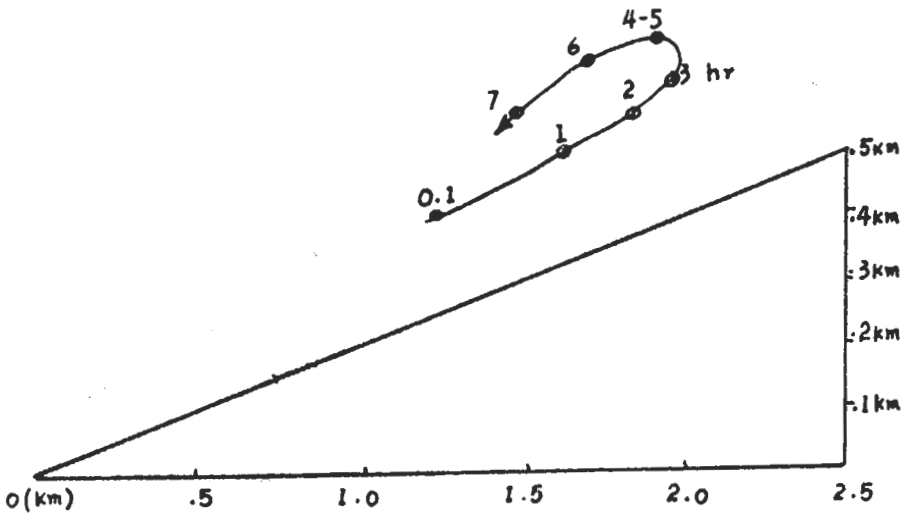

Fig. 3. Trajectory of the streamline center.
流線中心軌跡圖

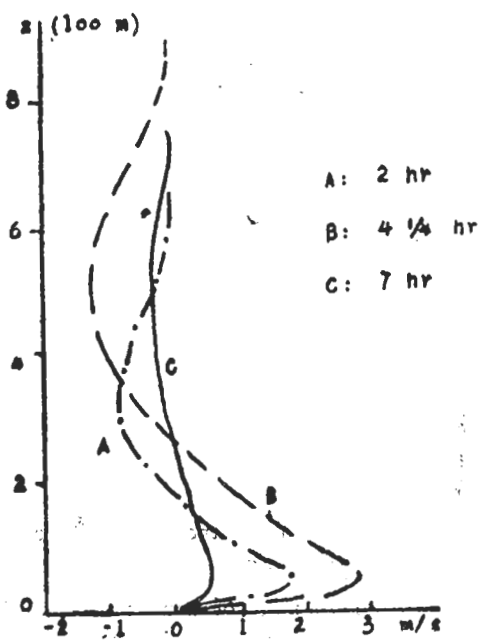

Fig. 4. Wind profile along the vertical of maximum upslope motion at t = 2 hr, 4 1/4 hr, and 7 hr.
最大上坡運動之垂直風剖影圖

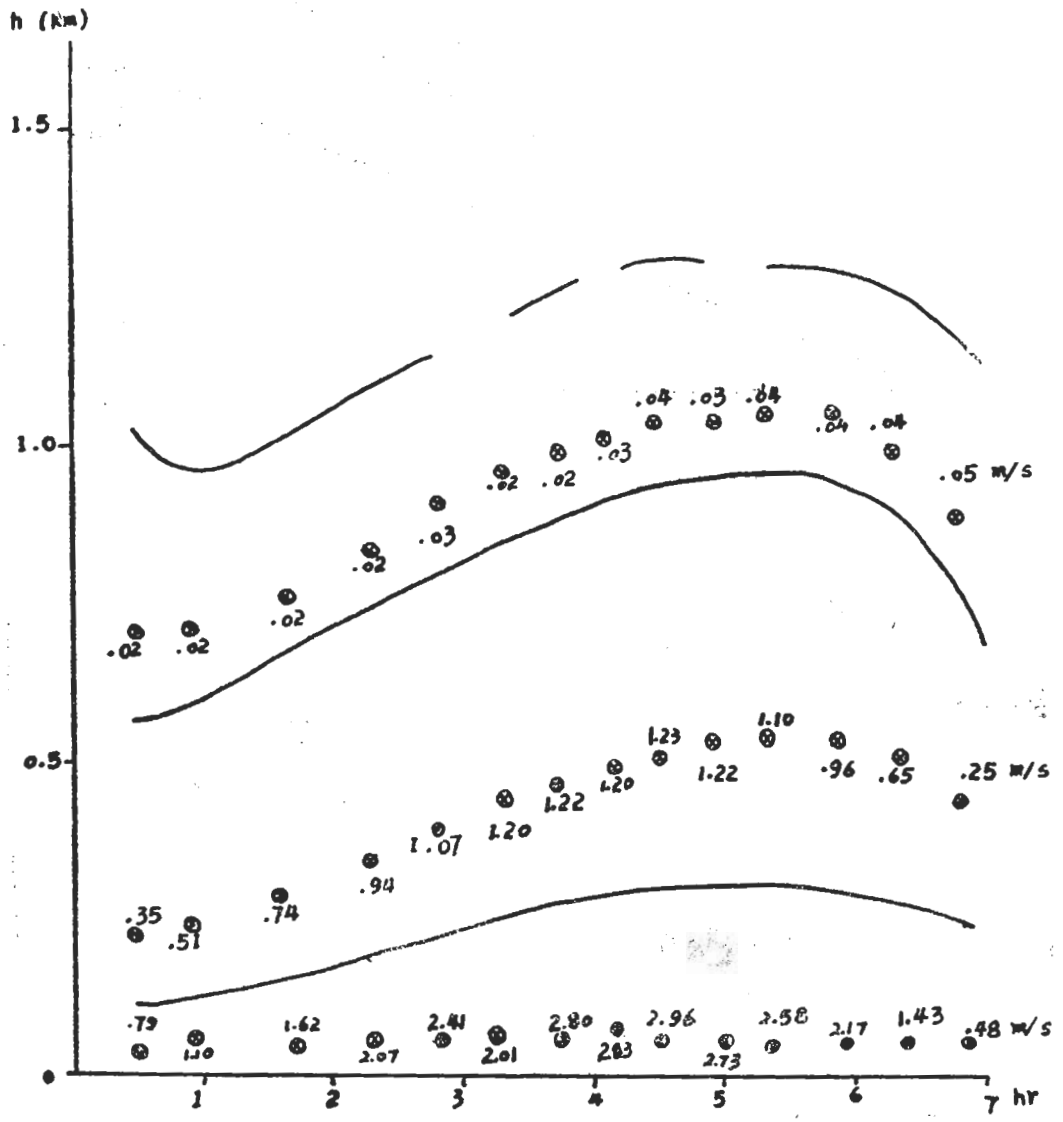

Fig. 5. Time variation of layered structure.
成層結構之時間變化圖
——where change of wind direction takes place
⊗ location and magnitude of maximum wind in the layer

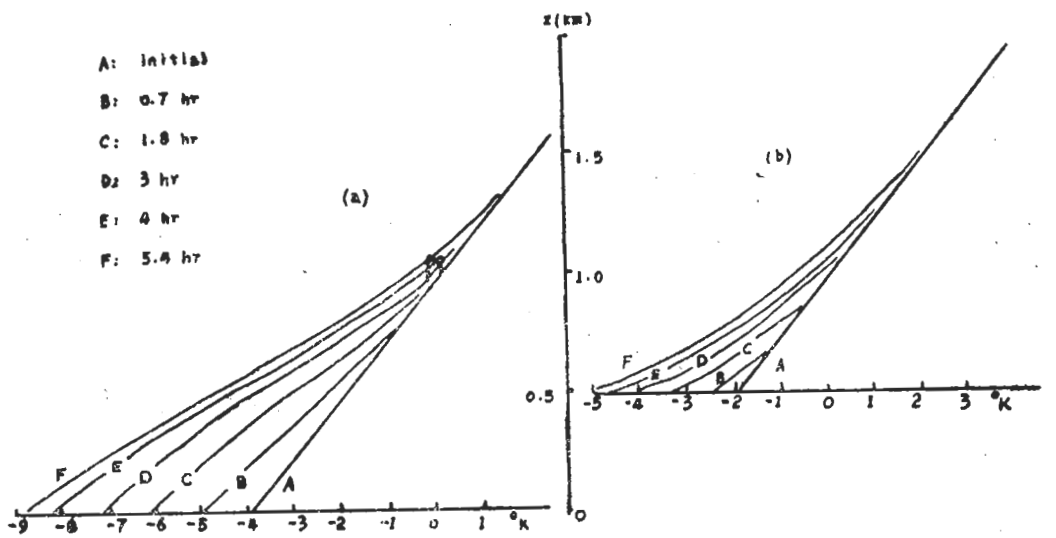

Fig. 6. Time variations of θ' profile over (a) the valley and (b) the ridge.
谷(a)及脊(b)上θ'之時間變化圖

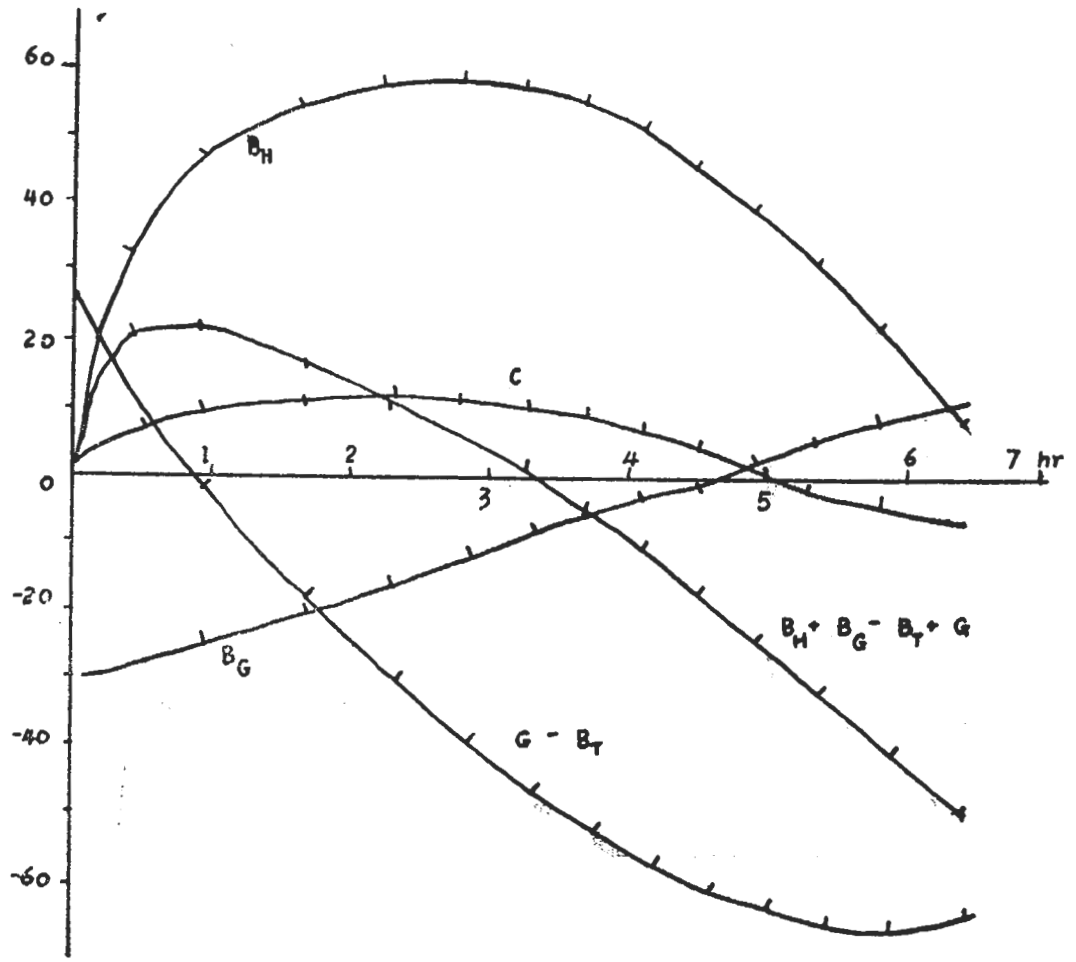

Fig. 7. Time variations of potential energy fluxes and transformation (in relative units)

位能流束及傳遞之時間變化圖

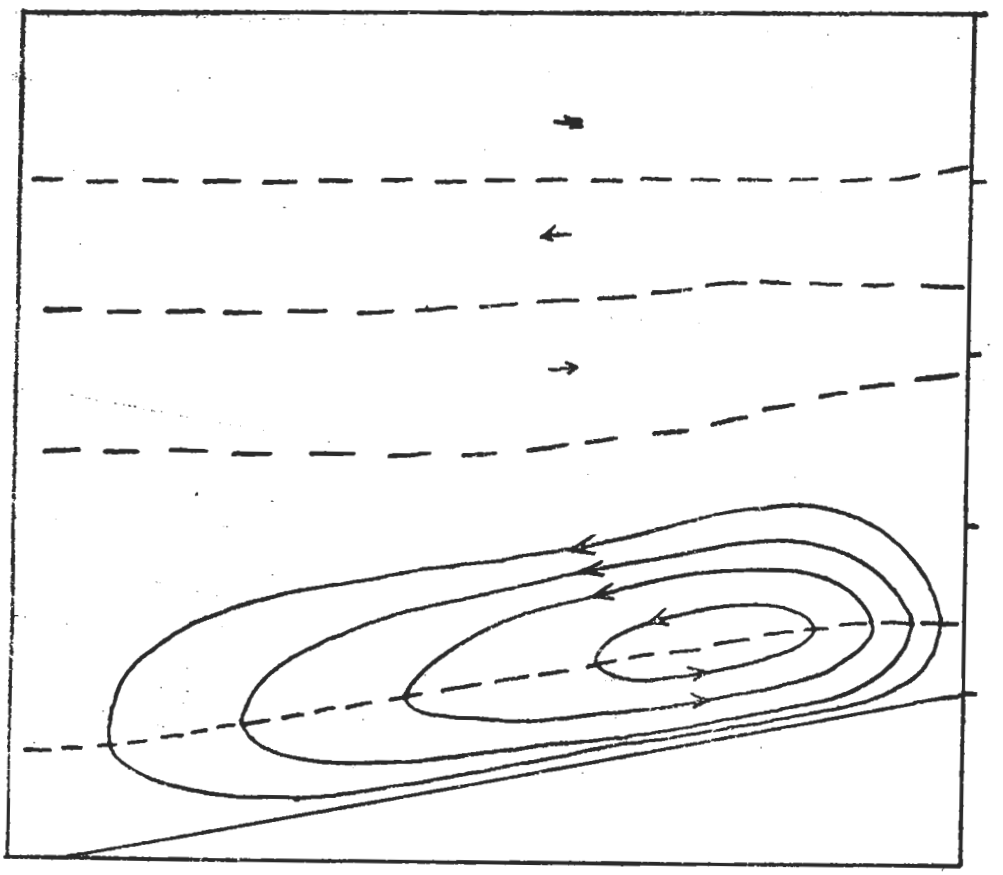

Fig. 8. Streamlines at $t = 4\ 1/4$ hr.

4 1/4小時時之流線圖

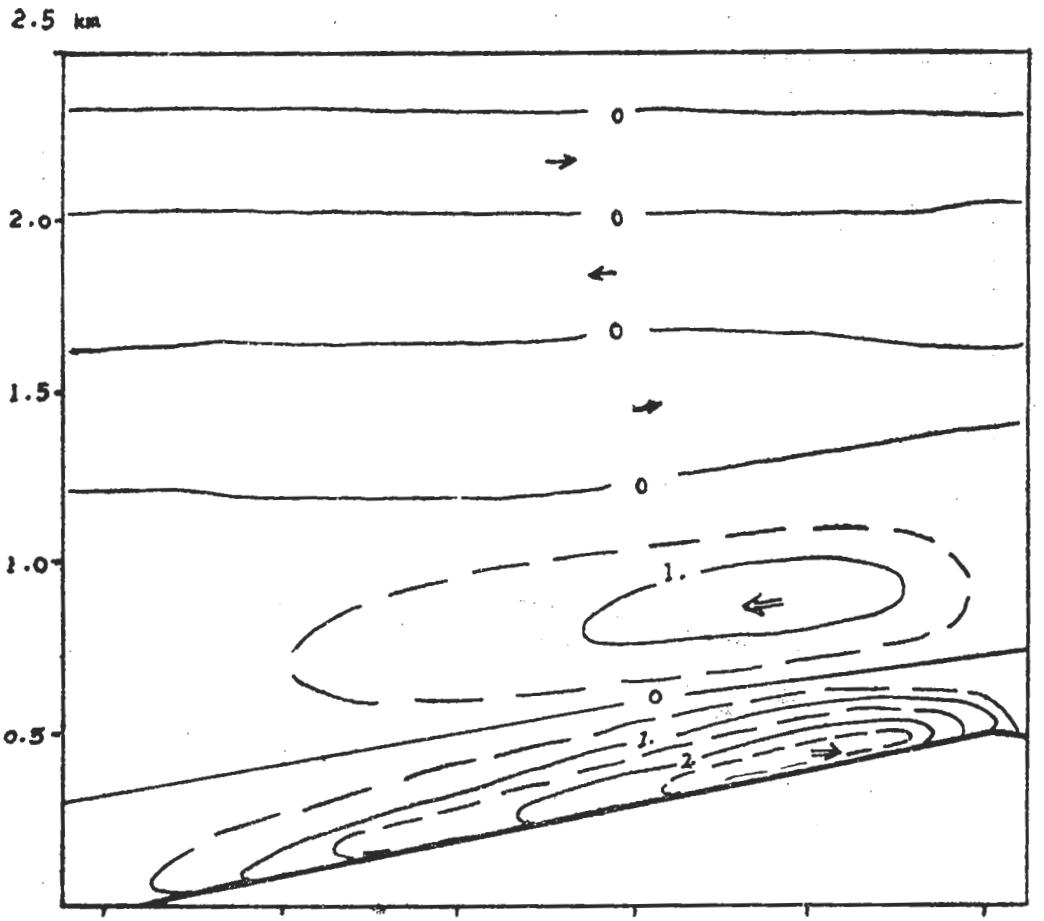

Fig. 9 Distrioution of horizontal velocity at t = 4 1/4 hr.

4 1/4 小時時水平速度分佈圖

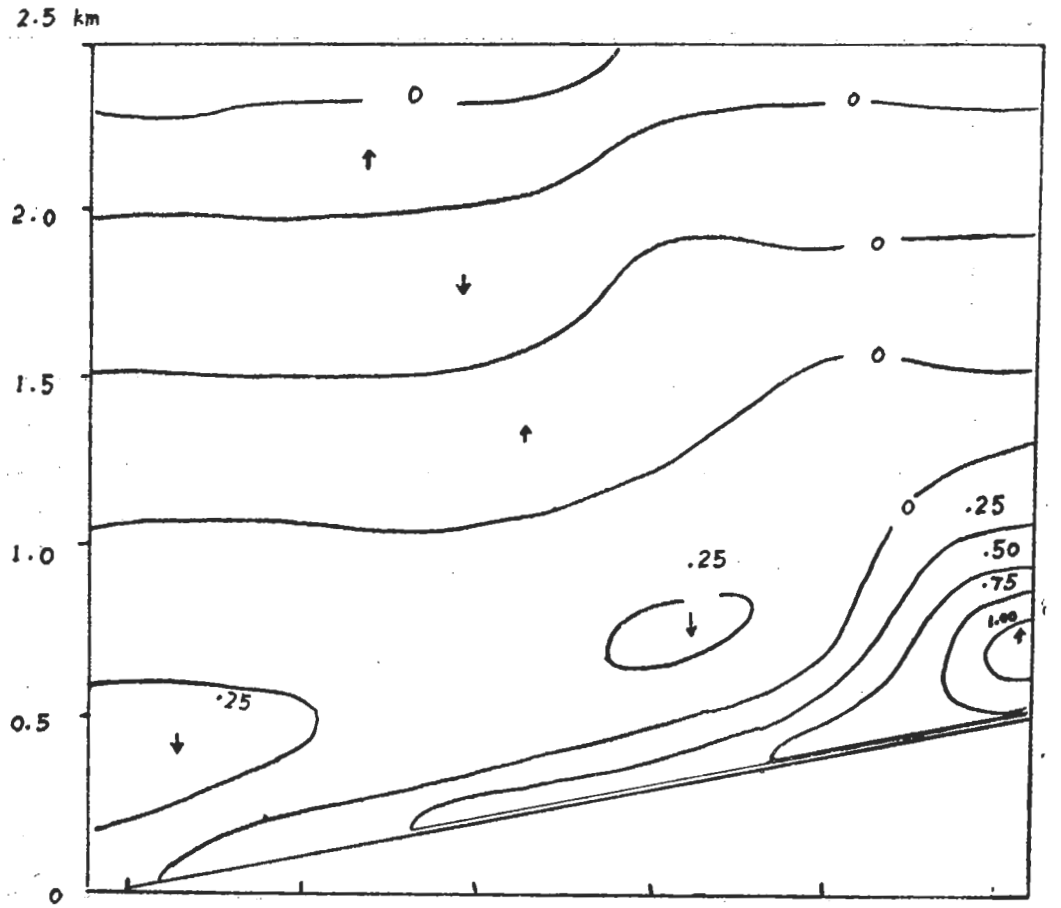

Fig. 10. Distribution of vertical velocity at t = 4 1/4 hr.

4 1/4 小時時垂直風速分佈圖

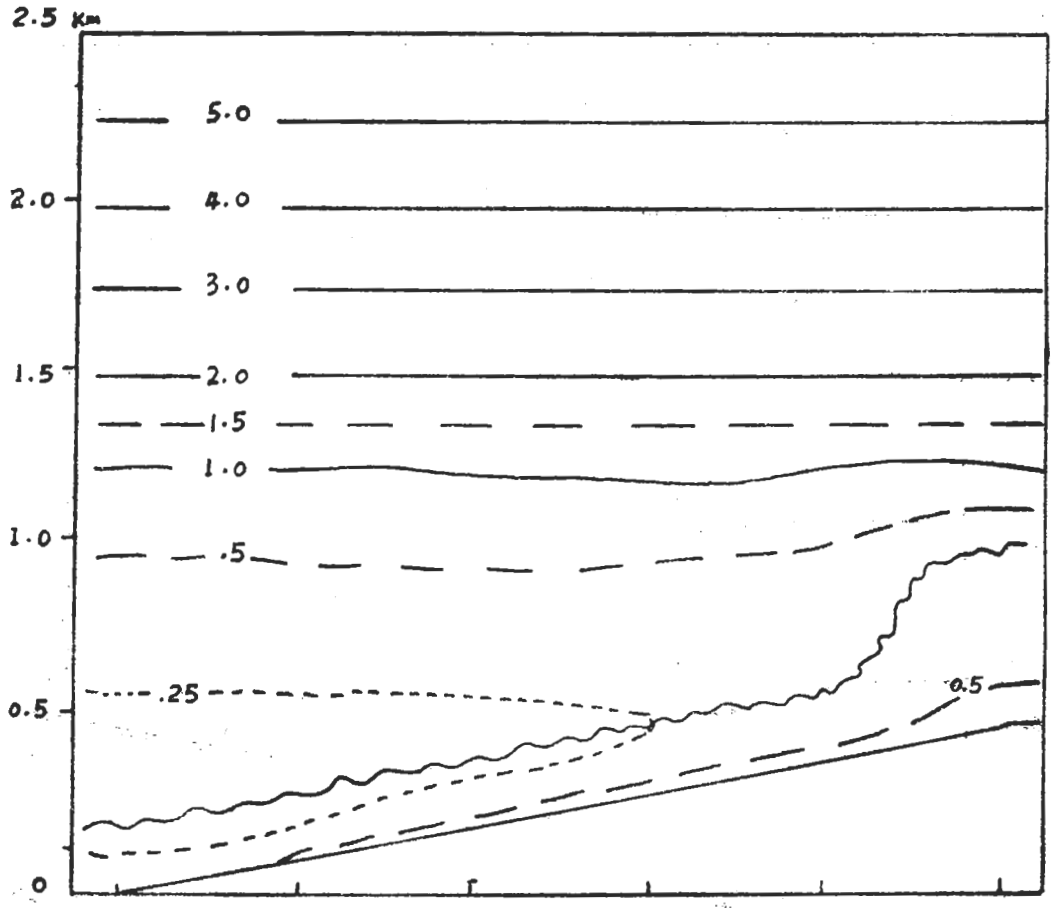

Fig. 11. Distrioution of θ' at t = 4 1/4 hr.

4 1/4 小時時θ'之分佈圖

~~~~top of the layer of super-adiabatic lapse rate.
~~~~

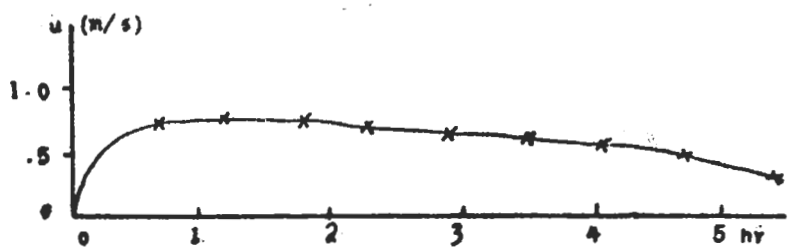

Fig. 12. Change of U_{max} with time.

U最大值隨時變化圖

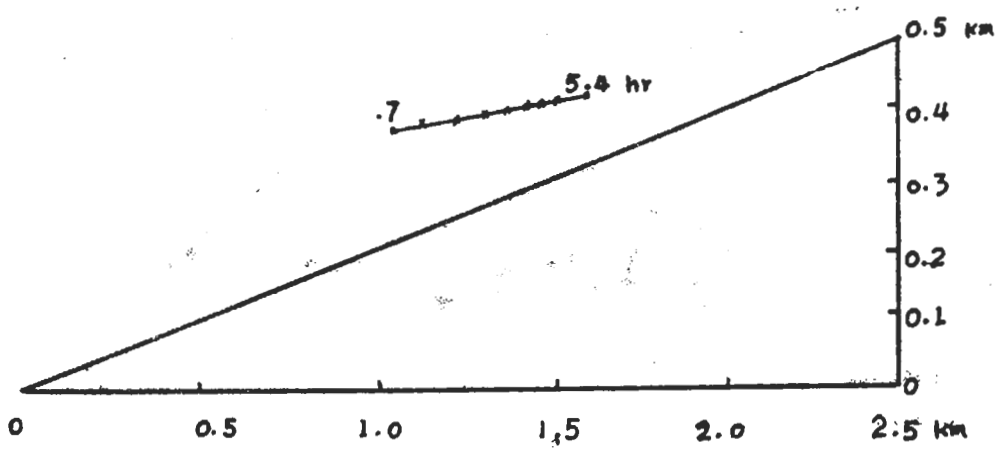

Fig. 13. Trajectory of the streamline center.

流線中心之軌跡圖

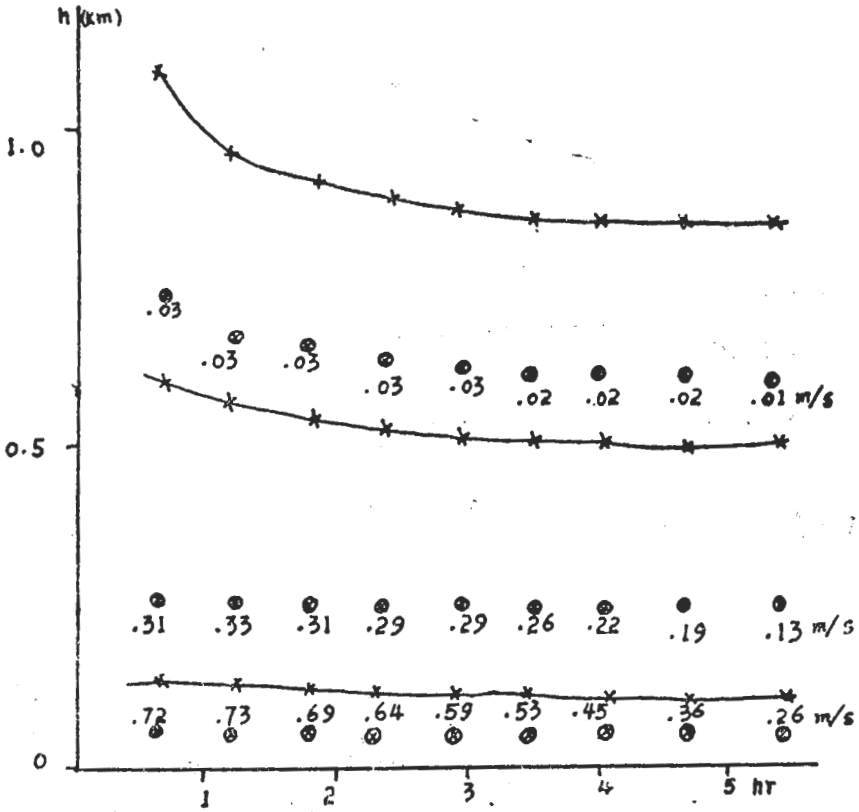

Fig. 14. Variation of layered structure of wind.
風之成層結構變化圖
——where change of wind direction takes place,
⊗ location and magnitude of maximum wind in the layer

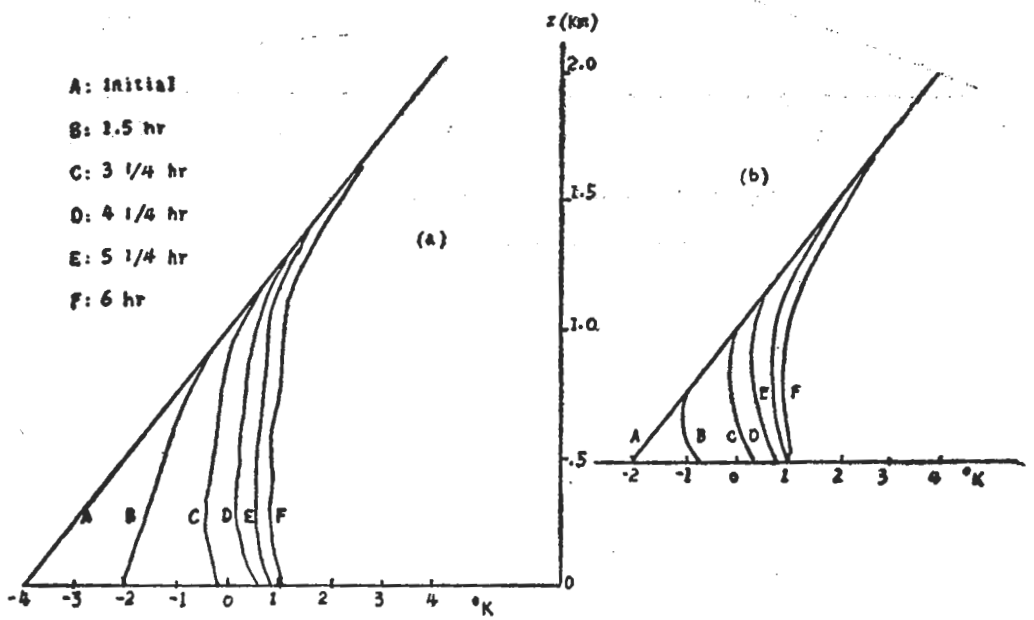

Fig. 15. Time variations of θ' profile over (a) the valley and (b) the ridge.
谷(a)及脊(b)上θ'剖影圖之時間變化圖